Nano Convergence

FULL PAPER

Open Access

Promoting N_2 electroreduction to ammonia by fluorine-terminating $Ti_3C_2T_x$ MXene

Yu Ding[1], Junbo Zhang[1], Anxiang Guan[1], Qihao Wang[1], Si Li[1], Abdullah M. Al-Enizi[2], Linping Qian[1], Lijuan Zhang[1*] and Gengfeng Zheng[1*]

Abstract

Two-dimensional MXene-based materials are potential of presenting unique catalytic performances of electrocatalytic reactions. The surface functionalization of MXene-based catalysts is attractive for developing efficient electrocatalysts toward nitrogen reduction reaction. Herein, we reported a $Ti_3C_2T_x$ MXene with a medium density of surface functionalized fluorine terminal groups, as an excellent N_2 reduction reaction electrocatalyst with enhanced adsorption and activation of N_2. The $Ti_3C_2T_x$ MXene catalyst showed a production rate of ammonia as 2.81×10^{-5} μmol·s^{-1}·cm^{-2}, corresponding to a partial current density of 18.3 μA·cm^{-2} and a Faradic efficiency of 7.4% at − 0.7 V versus reversible hydrogen electrode in aqueous solutions at ambient conditions, substantially exceeding similar $Ti_3C_2T_x$ MXene catalysts but with higher or lower densities of surface fluorine terminal groups. Our work suggests the capability of developing surface functionalization toolkit for enhancing electrochemical catalytic activities of two-dimensional MXene-based materials.

Keywords: MXene, Surface functionalization, Electrocatalysis, N_2 reduction reaction, Fluorine

1 Introduction

Artificial nitrogen fixation to ammonia (NH_3) plays a critical role in fabricating agricultural fertilizers and maintaining the earth's ecosystems [1–3]. The traditional NH_3 synthesis in industry depends heavily on the Haber–Bosch process with high temperatures of 350–550 ℃ and pressures of 150–350 atm [4, 5]. In recent years, new strategies, such as biological [6], photocatalytic [7] and electrocatalytic [8–10] approaches, have been reported for ammonia synthesis. In particular, electrocatalytic nitrogen reduction reaction (N_2RR) can use water as hydrogen source and proceed in ambient conditions, suggesting an attractive feature of clean ammonia production with low carbon footprint [11]. Nevertheless, the development of N_2RR has been largely limited by its low current densities, limited Faradaic efficiency (FE) values, and slow NH_3 production rates, which are ascribed to the large reaction energy barriers during NH_3 adsorption and activation processes [12]. It is critical to design robust electrocatalysts that can efficiently adsorb, activate and convert N_2 into NH_3.

Two-dimensional (2D) materials, such as graphene [13], metal–organic frameworks [14], black phosphorus [15], have been drawing great attention of researchers for N_2RR, owning to their unique 2D structures and unconventional chemical properties [16]. MXenes, one of the novel 2D materials synthesized by selective etching of the aluminum layers from the precursor MAX phases [17], have been demonstrated with applications in supercapacitors [18], batteries [19], and electrochemical N_2RR [20–22]. For instance, Luo et al. [23] reported that $Ti_3C_2T_x$ MXene on stainless steel mesh functioned as efficient N_2RR electrocatalysts with a FE of 5.78%. On the other hand, the terminal groups (T_x), mainly oxygen (O)-containing or fluorine (F)-terminations, can be tuned to affect the electrocatalytic performances of $Ti_3C_2T_x$ MXene [24]. Previously, density functional theory (DFT)

*Correspondence: zhanglijuan@fudan.edu.cn; gfzheng@fudan.edu.cn
[1] Laboratory of Advanced Materials, Department of Chemistry, Faculty of Chemistry and Materials Science, Fudan University, Shanghai 200438, China
Full list of author information is available at the end of the article

calculations suggested that Ti_3C_2 MXene with O-containing terminal groups can combine N_2 more strongly than that with F-terminal groups [25]. The bond length of N_2 for Ti_3C_2 MXene with F-terminal groups was calculated to be slightly larger than that with O-containing terminal groups [26]. The computational calculations also indicated that a moderate proportion of F-termination on $Ti_3C_2T_x$ MXene was theoretically beneficial to the adsorption and electrocatalytic activation of nitrogen. Thus, efforts are needed to develop efficient and tunable functionalization on the surface of $Ti_3C_2T_x$ MXene to optimize its N_2RR performance and achieve highly selective NH_3 production.

Herein, we developed the surface modification of MXene-based catalysts to optimize the N_2RR performance. The fluorine-terminal groups on the MXene surface were modified by treating with different concentrations of fluorine-containing acids and subsequent alkalization. Due to the combined effects including hydrogenation and N_2 activation, $Ti_3C_2T_x$ MXene with a medium F-terminal group density (designated as $Ti_3C_2T_x$-medium F) exhibited the optimal electrocatalytic N_2RR performances. The NH_3 production rate was 2.81×10^{-5} μmol·s^{-1}·cm^{-2} in 0.01 M Na_2SO_4 electrolyte at − 0.7 V versus reversible hydrogen electrode in ambient conditions, corresponding to a FE of 7.4% and a partial current density up to 18.3 μA·cm^{-2}.

2 Experimental

$Ti_3C_2T_x$ MXene nanosheets were synthesized via a fluorine-containing etching method [27, 28], which selectively etched the Al layers in Ti_3AlC_2 with fluorine-containing acid, followed by exfoliating steps to obtain $Ti_3C_2T_x$ MXene nanosheets. To modify the density of fluorine terminal groups on the surface of $Ti_3C_2T_x$ MXene, different fluorine-containing acids were used. In brief, 2 g of LiF was dissolved in 20 mL of 6 M HCl solution, and stirred for 5 min to form a high fluorine-containing acid environment to prepare the $Ti_3C_2T_x$ MXene with high surface density of F-terminal groups; while 20 mL of 10% hydrofluoride acid (HF) was used to obtain a medium surface density of F-terminal groups. In order to further reduce the fluorine ratio of the terminal groups on the MXene surface, $Ti_3C_2T_x$ MXene with medium density of fluorine-terminal groups was immersed into 0.5 M KOH solution to replace fluorine terminal groups by hydroxyl groups.

In our experiments, 1 g of Ti_3AlC_2 MAX precursor was slowly added into the aforementioned solutions respectively, and the obtained mixture was stirred for 24 h at room temperature to achieve different surface functionalization of fluorine or hydroxyl groups. Afterwards, the resulting solution was washed with deionized (DI) water and centrifuged at 3500 rpm for several times until pH of the solution was 6–7. To prepare few-layer $Ti_3C_2T_x$ MXene nanosheets, the sediment was then dispersed in DI water and ultrasonicated for 30 min in ice bath with Ar gas bubbling. The few-layer $Ti_3C_2T_x$ MXene solution was then obtained by centrifugation at 3500 rpm for 30 min. A polyvinyl difluoride (PVDF) membrane was utilized to filter $Ti_3C_2T_x$ MXene product and the obtained powder was dried with membrane for 12 h at room temperature.

3 Results and discussion

The synthesis process of $Ti_3C_2T_x$ MXene nanosheets included two successive steps [27, 28]: selective etching of aluminum (Al) layer on MAX phases with a fluorine-containing etching method, and delaminating of MXene layers by sonication (Fig. 1a). After these two steps of preparation, the original structure of Ti_3AlC_2 MAX phase (Additional file 1: Fig. S1) was transformed into few-layer, 2-dimensional $Ti_3C_2T_x$ MXene (Fig. 1b). The surface of $Ti_3C_2T_x$ MXene was covered by different terminal groups, mainly including O-containing groups (e.g.–O, − OH) and fluorine groups [29]. Energy-dispersive X-ray spectroscopy (EDS) elemental mapping analysis showed that Ti, C, O, and F elements were evenly distributed on the obtained $Ti_3C_2T_x$ MXene (Fig. 1c). The color of few-layer $Ti_3C_2T_x$ MXene appeared as a blackish green color instead of pure black (Additional file 1: Fig. S2a), and the Tyndall scattering effect was also observed (Additional file 1: Fig. S2b). These two empirical phenomena indicated the formation of few-layer, sheet-like structure of $Ti_3C_2T_x$ MXene.

The X-ray powder diffraction (XRD) pattern exhibited the characteristic peaks of $Ti_3C_2T_x$ MXene, which differed greatly from the Ti_3AlC_2 MAX precursor (Fig. 1d). After etching, the peak ($2\theta \approx 9.28°$) on Ti_3AlC_2 MAX phase exhibited a negative shift to a low angle ($2\theta \approx 5.89°$), corresponding to the characteristic lattice (002) plane of $Ti_3C_2T_x$ MXene [30]. No additional peaks were observed for $Ti_3C_2T_x$ MXene except for the peaks of carbon paper. The differences of the XRD patterns between $Ti_3C_2T_x$ MXene and Ti_3AlC_2 MAX indicated the successful etching of Al layers from Ti_3AlC_2 MAX phases.

Scanning electron microscopy (SEM) images showed that all the synthesized $Ti_3C_2T_x$ MXene were 2D sheet-like structures (Additional file 1: Fig. S3). The ratio of F-terminal groups to all the surface groups of $Ti_3C_2T_x$ MXene was measured by EDS profiles (Additional file 1: Fig. S4), which was calculated as 82% (designated as $Ti_3C_2T_x$-high F, indicating that it was etched by a high-concentration fluorinated acid) and 48% (designated as $Ti_3C_2T_x$-medium F, indicating that it was etched by a medium-concentration fluorinated acid). To further

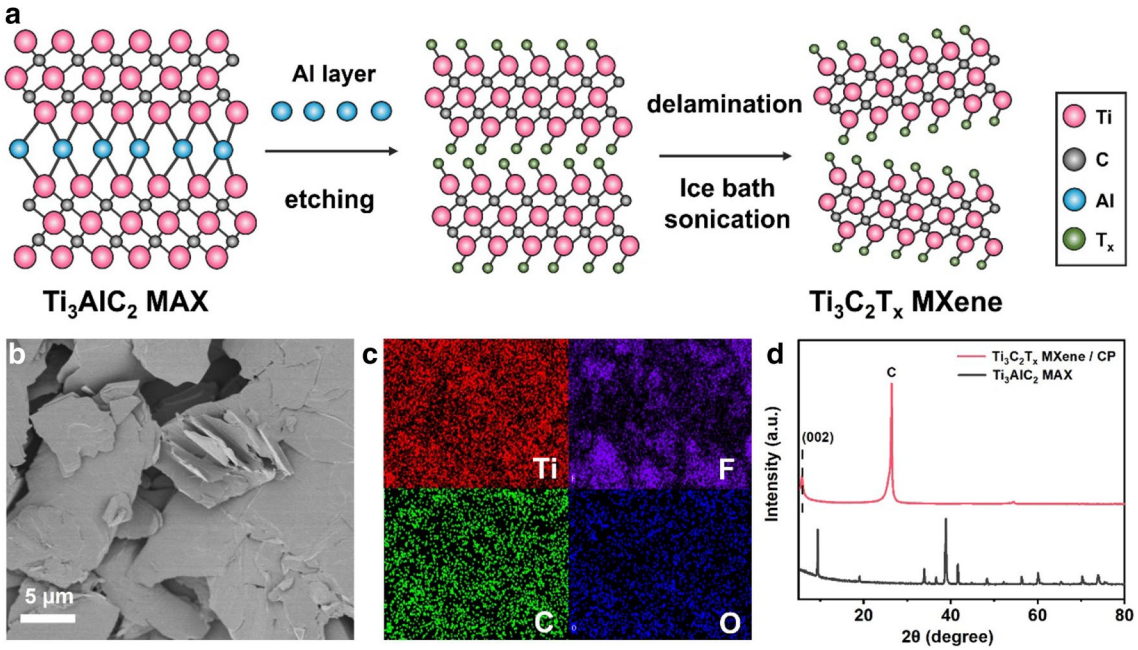

Fig. 1 **a** Schematic of the synthesis procedure of the $Ti_3C_2T_x$ MXene. **b** SEM images of $Ti_3C_2T_x$ MXene. **c** EDX elemental mapping profiles of $Ti_3C_2T_x$ MXene with Ti (red), F (purple), C (green), and O (blue) distributions. **d** XRD spectra of $Ti_3C_2T_x$ MXene loaded on carbon paper (CP)

decrease the ratio of fluorine groups on the surface of MXene, an alkalization treatment was conducted to $Ti_3C_2T_x$-medium F MXene (Experimental section), and the fluorine proportion was reduced to 24% (designated as $Ti_3C_2T_x$-low F).

To investigate the structures of $Ti_3C_2T_x$ MXene with different amounts of fluoride, Raman and X-ray photoelectron spectroscopy (XPS) were conducted to qualitatively investigate the fluorine ratio in all the terminal groups. As shown in the Raman spectra (Fig. 2a), the relative intensity of vibrational modes for $Ti_3C_2T_x$ indicated the densities of terminal groups on MXene. The Raman shifts at 205 and 366 cm^{-1} were respectively associated to the A_{1g} and E_g vibration modes of the C–Ti–O structure. The Raman peak at 614 cm^{-1} corresponded to the C–Ti–OH structure [23], and the Raman peak at 706 cm^{-1} represented the A_{1g} vibrations of carbon. The relatively large intensity of the characteristic Raman peaks at 205, 614, and 366 cm^{-1} corresponded to the O-containing terminal groups, and suggested that the densities of O-terminal groups were in the order of $Ti_3C_2T_x$-low F > $Ti_3C_2T_x$-medium F > $Ti_3C_2T_x$-high F. This trend also confirmed that the densities of F-terminal groups followed the order as: $Ti_3C_2T_x$-high F > $Ti_3C_2T_x$-medium F > $Ti_3C_2T_x$-low F.

The survey XPS spectra of all the $Ti_3C_2T_x$ MXene samples with different densities of fluorine terminal groups exhibited same element peaks (Fig. 2b), which assigned to F 1 s, O 1 s, Ti 2p and C 1 s, respectively. Among these samples, $Ti_3C_2T_x$ MXene-high F showed the highest intensity of F 1 s and the lowest intensity of O 1 s, indicating the highest ratio of fluorine terminal groups among these samples, in good accord with the EDX result. The F 1 s XPS spectra presented two main peaks at 684.5 and 685.9 eV (Fig. 2c), corresponding to the F–Ti and F–C bonds, respectively. For the O 1 s spectra (Additional file 1: Fig. S5), the peaks at 529.3, 531.2 and 533.4 eV were ascribed to C–Ti–O, C–Ti–OH species, and the adsorbed H_2O on the MXene surface. With the increased concentrations of alkali solutions, the density of C–Ti–O species on the MXene surface increased and the fluorine terminal groups decreased. For the Ti 2p XPS spectrum (Fig. 2d), four doublets were fitted to indicate the valance and bond structures of Ti. The peaks centered at 454.4 and 460.6 eV referred to Ti^{3+}; the peaks at 455.0 and 461.7 eV were assigned to Ti^{2+}; the peaks at 456.2 and 462.9 eV were associated with the Ti—C bond; the peaks at 458.4 and 464.3 eV were ascribed to the Ti—O bond; and the peak at 459.5 eV was attributed to the Ti—F bond. The relative intensities of Ti—O and Ti—F bonds also indicated that the fluorine terminal group density on the MXene surface followed the order of $Ti_3C_2T_x$-high F > $Ti_3C_2T_x$-medium F > $Ti_3C_2T_x$-low F.

The capability of different F-terminating surface functionalizations of $Ti_3C_2T_x$ MXene for enhancing the N_2RR catalytic activity was then investigated. All the

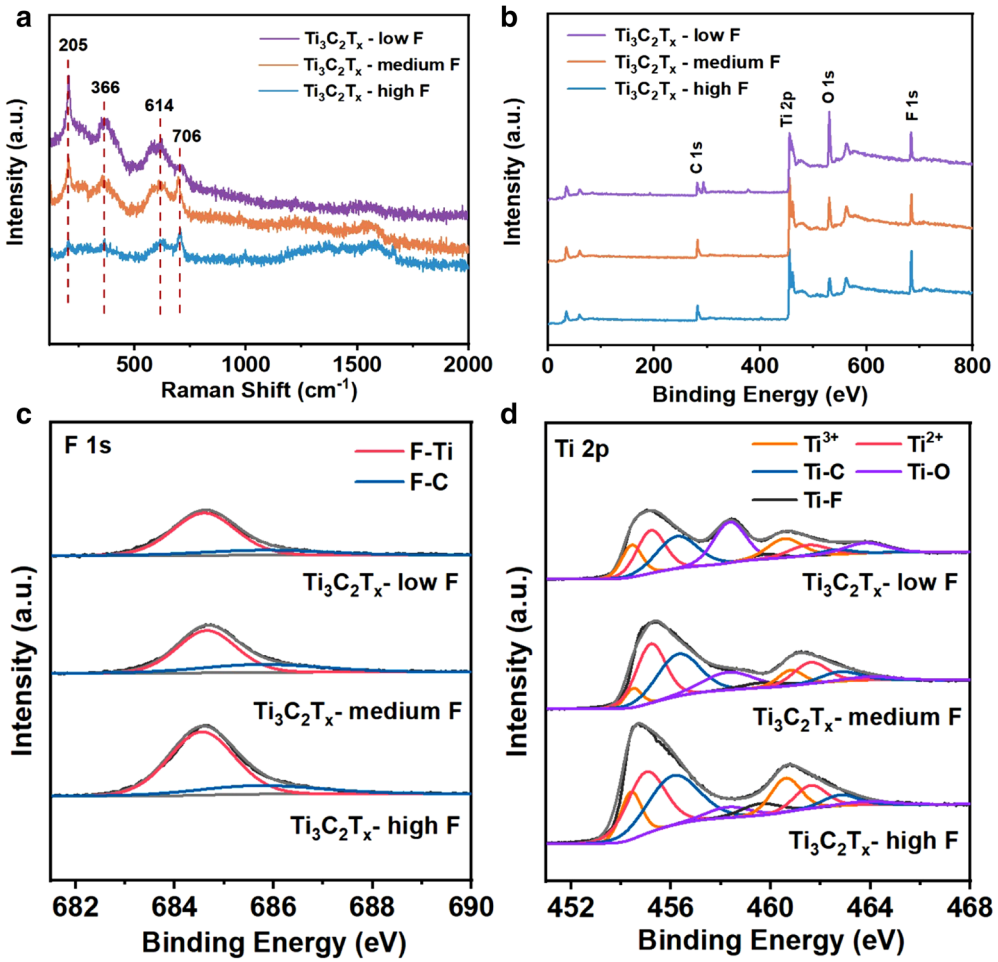

Fig. 2 **a** Raman spectra and **b** XPS spectra of $Ti_3C_2T_x$-low F, $Ti_3C_2T_x$-medium F and $Ti_3C_2T_x$-high F. **c** F 1 s spectra, and **d** Ti 2p XPS spectra of $Ti_3C_2T_x$-low F, $Ti_3C_2T_x$-medium F and $Ti_3C_2T_x$-high F MXene samples

electrochemical tests were conducted in N_2-saturated 0.01 M Na_2SO_4 electrolyte, and all the potentials presented in this work were converted as values versus reversible hydrogen electrode (RHE). The linear sweep voltammetry (LSV) curves of $Ti_3C_2T_x$ MXene with different proportions of fluorine terminal groups were recorded (Fig. 3a). The experimental overpotentials of $Ti_3C_2T_x$ MXene displayed the following order of $Ti_3C_2T_x$-high F > $Ti_3C_2T_x$-medium F > $Ti_3C_2T_x$-low F at -10 mA·cm^{-2} current density, which was associated with the hydrogenation step during electrochemical reduction. Owning to the different densities of F-termination on the MXene surface, the hydrogenation step could be inhibited [31]. The $Ti_3C_2T_x$-high F sample had the highest density of fluorine terminal groups, resulting in the inhibition of H^+ adsorption [32] and eventually the decline of N_2RR activity. In contrast, $Ti_3C_2T_x$-low F had a low density of fluorine terminal groups and abundant O-containing termination, and presented the highest hydrogen evolution reaction (HER) performance but low N_2 adsorption and activation capabilities. In comparison, $Ti_3C_2T_x$-medium F MXene had a medium density of fluorine terminal groups, and presented the highest N_2RR electrocatalytic activity.

The $Ti_3C_2T_x$-medium F MXene catalyst was further tested in both Ar-saturated and N_2-saturated electrolytes (Fig. 3b). The current density in N_2-saturated electrolyte (red curve) exceeded that in Ar-saturated electrolyte (black curve) in the voltage range between -0.4 and -0.8 V, indicating the occurrence of electrochemical N_2RR on the catalyst surface. Both the chronoamperometric tests and the salicylic acid indicator method were adopted to determine the amount of produced NH_3. All the yields of ammonia were calculated from the standard curves (Additional file 1: Fig. S6). In addition, each experiment was also conducted in Ar-saturated electrolyte to serve as the background. The corrected rate of NH_3 yield ($YR_{corrected}$) was calculated from the following

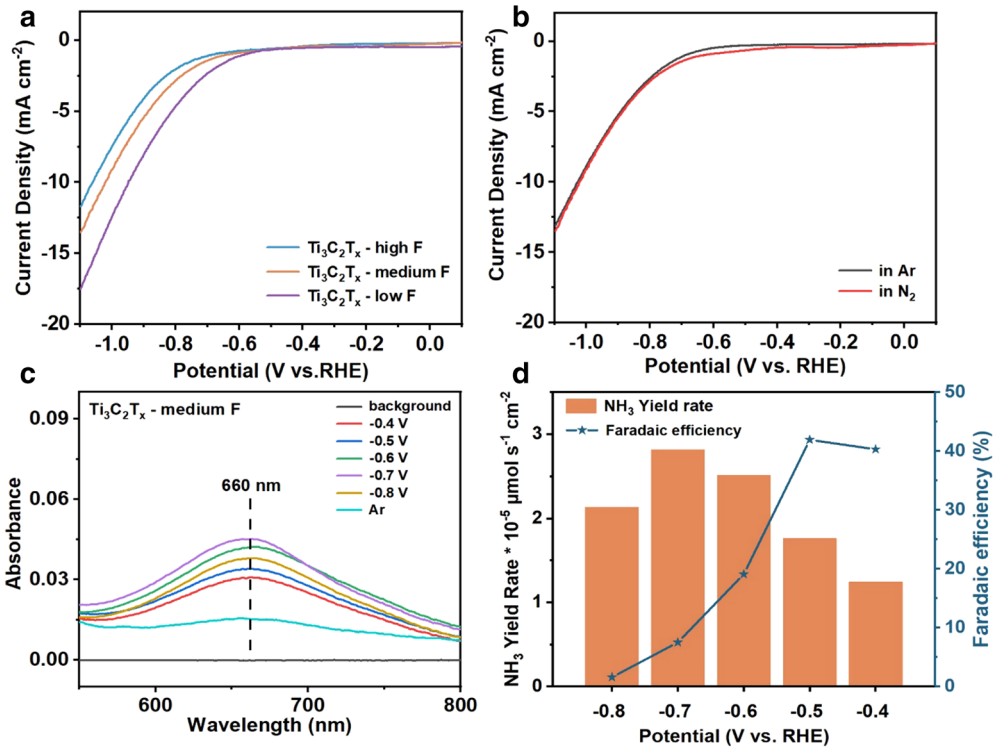

Fig. 3 **a** Linear sweep voltametric curves of $Ti_3C_2T_x$-low F, $Ti_3C_2T_x$-medium F and $Ti_3C_2T_x$-high F in N_2-saturated 0.01 M Na_2SO_4 electrolyte with a scan rate of 5 mV·s^{-1}. **b** LSV curves of $Ti_3C_2T_x$-medium F in N_2-saturated (red curve) and Ar-saturated (black curve) 0.01 M Na_2SO_4 electrolyte with a scan rate of 5 mV·s^{-1}. **c** UV–Vis absorption spectra of N_2RR products of $Ti_3C_2T_x$-medium F at potentials between –0.4 and –0.8 V over $Ti_3C_2T_x$ -48% F. **d** NH_3 yield rate (left y-axis) and Faradaic efficiencies (right y-axis) of $Ti_3C_2T_x$-medium F MXene at the corresponding potentials

equation: $YR_{corrected} = YR_{N2} - YR_{Ar}$. The NH_3 yield rate from $Ti_3C_2T_x$-medium F MXene was calculated based on the corresponding UV–Vis absorption spectra at the potential range between –0.4 and –0.8 V (Fig. 3c). The value of average background (YR_{Ar}) was calculated as $(2.03 \pm 0.2) \times 10^{-5}$ μmol·s^{-1}·cm^{-2}. As shown in Fig. 3d, the maximum FE for NH_3 production by $Ti_3C_2T_x$-medium F MXene was 42.7% at –0.5 V, while the highest NH_3 partial current density after background correction was 18.3 μA·cm^{-2} at –0.7 V, corresponding to an FE of 7.4% and the NH_3 production rate of 2.81×10^{-5} μmol·s^{-1}·cm^{-2}.

The chronoamperometry curves and the corresponding UV–Vis absorption spectra over $Ti_3C_2T_x$ MXene with different densities of F-terminal groups at all applied potentials were displayed (Additional file 1: Fig. S7). Compared to $Ti_3C_2T_x$ MXene counterparts with higher or lower surface densities of fluorine terminal groups (i.e., $Ti_3C_2T_x$-high F and $Ti_3C_2T_x$-low F), the $Ti_3C_2T_x$-medium F MXene catalyst covered with medium fluorine terminal group density exhibited the highest N_2RR catalytic performance (Fig. 4a, b). The corrected NH_3 yield rate ($YR_{corrected}$) with $Ti_3C_2T_x$-medium F catalyst (2.81×10^{-5} μmol·s^{-1}·cm^{-2}) was 1.6 and 1.7 times higher than that of $Ti_3C_2T_x$-high F (1.75×10^{-5} μmol·s^{-1}·cm^{-2}) and $Ti_3C_2T_x$-low F (1.67×10^{-5} μmol·s^{-1}·cm^{-2}) at –0.7 V.

The electrochemical stability of the $Ti_3C_2T_x$-medium F MXene catalyst was further interrogated. As shown in Fig. 4c, the total electrolysis current density in N_2-saturated electrolyte was maintained relatively stable over 18 h. Moreover, cycling test of six continuous times was conducted, and the corresponding chronoamperometric measurements and UV–Vis absorption spectra were examined after each cycle (Additional file 1: Fig. S7e, f). Both of NH_3 production rate ($2.67 \pm 0.16 \times 10^{-5}$ μmol·s^{-1}·cm^{-2}) and the FE values ($7.5\% \pm 0.5\%$) were within the error range of 7.4% after the continuous chronoamperometric measurement for 6 times, with 1 h of measurement each time (Fig. 4d), which suggesting the excellent durability of $Ti_3C_2T_x$-medium F MXene. Furthermore, the XRD patterns of $Ti_3C_2T_x$ MXene before and after electrochemical nitrogen reduction reaction were also displayed (Additional file 1: Fig. S8), the unvaried peak position of XRD patterns also testified the stable crystal phases and structure of $Ti_3C_2T_x$ MXene. Thus, $Ti_3C_2T_x$-medium F MXene with a medium density of

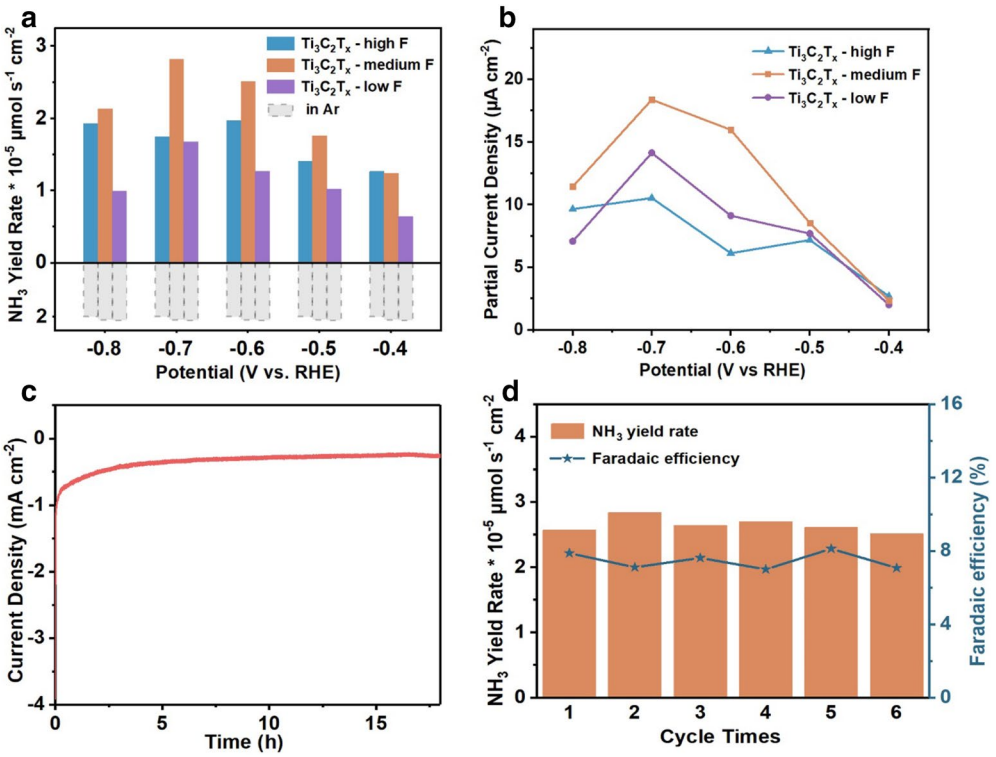

Fig. 4 **a** The ammonia production rates and **b** partial current densities of NH_3 production of $Ti_3C_2T_x$ MXene samples with different surface densities of fluorine terminal groups. **c** Chronoamperometry curve of $Ti_3C_2T_x$-medium F MXene for 18 h under –0.7 V. **d** The NH_3 yield rate (left y-axis) and Faradaic efficiency (right y-axis) of $Ti_3C_2T_x$-medium F MXene at –0.7 V for 6 times

surface fluorine terminal groups was demonstrated as an optimal catalyst for N_2RR.

4 Conclusions

In summary, we demonstrated the surface functionalization of fluorine terminal groups on MXene to tune the N_2RR catalytic activity at ambient conditions, in which different densities of surface fluorine terminal groups allowed to affect the capability of N_2 adsorption and activation. The $Ti_3C_2T_x$ MXene catalyst with a medium F-termination proportion ($Ti_3C_2T_x$-medium F) showed the optimal N_2RR activity, with the highest NH_3 yield rate of 2.81×10^{-5} μmol·s^{-1}·cm^{-2} at –0.7 V, substantially exceeding that of $Ti_3C_2T_x$-high F and $Ti_3C_2T_x$-low F. Further study and development of surface functionalization toward N_2 adsorption and activation can serve as a powerful toolkit for improving artificial N_2 fixation.

Supplementary Information

The online version contains supplementary material available at https://doi.org/10.1186/s40580-021-00264-9.

Additional file 1: **Fig. S1**. (a-c) SEM images and (d) EDS elemental analysis profile of Ti3AlC2 MAX. **Fig. S2**. (a) The blackish green color and (b) the Tyndall scattering effect of Ti3C2Tx MXene solution. **Fig. S3**. SEM images of (a-c) Ti3C2Tx-high F; (d-f) Ti3C2Tx-medium F and (g-i) Ti3C2Tx-low F. **Fig. S4**. EDS elemental analysis profiles of (a) Ti3C2Tx-low F; (b) Ti3C2Tx-medium F (c) Ti3C2Tx-high F, and (d) the element analysis of all MXene samples. **Fig. S5**. (a) O 1s and (b) C 1s XPS spectra of Ti3C2Tx-low F, Ti3C2Tx-medium F and Ti3C2Tx-high F Mxene samples. **Fig. S6**. (a) UV-Vis absorption spectra of standard ammonia solutions with salicylic acid indicator. (b) Standard curves for determination of ammonia concentrations: y = 0.5408x – 0.0035, R2 = 0.995. **Fig. S7**. (a, c) Chronoamperometry curves of N2RR in 0.01 M Na2SO4 solution at corresponding potentials: (a) Ti3C2Tx-high F and (c) Ti3C2Tx-low F. (b, d) UV-Vis absorption spectra of (b) Ti3C2Tx-high F and (d) Ti3C2Tx-low F after N2RR electrolysis at different potentials for 1 h. (e) Chronoamperometry curves and (f) UV-Vis absorption spectra of N2RR over Ti3C2Tx-medium F at the potential of −0.7 V for 6 times. **Fig. S8**. XRD patterns of Ti3C2Tx MXene (on carbon paper, CP) before and after electrochemical nitrogen reduction reaction at the potential of −0.7 V. **Table S1**. Comparison of the electrochemical N2RR performances for MXene-based catalysts.

Acknowledgements
Not applicable.

Authors' contributions
GZ and LZ proposed, designed, and supervised the project. GZ, LZ, and YD wrote the manuscript. YD, JZ, AG, QW, SL, AMA and LQ performed the experiments and analyzed the data. All authors read and approved the final manuscript.

Funding
We thank the following funding agencies for supporting this work: the National Key Research and Development Program of China (2017YFA0206901, 2018YFA0209401), the National Science Foundation of China (22025502, 21975051, 21773036), the Science and Technology Commission of Shanghai Municipality (19XD1420400), and the Innovation Program of Shanghai Municipal Education Commission (2019–01-07–00-07-E00045). The authors also extend sincere appreciation to Researchers Supporting Project number (RSP-2021/55), King Saud University, Riyadh, Saudi Arabia for funding this research.

Availability of data and materials
The datasets used and/or analyzed during the current study are available from the corresponding author on reasonable request.

Declarations

Competing interests
The authors declare that they have no competing interests.

Author details
[1] Laboratory of Advanced Materials, Department of Chemistry, Faculty of Chemistry and Materials Science, Fudan University, Shanghai 200438, China. [2] Department of Chemistry, College of Science, King Saud University, Riyadh 11451, Saudi Arabia.

Received: 26 February 2021 Accepted: 7 April 2021
Published online: 10 May 2021

References

1. J.G. Chen, R.M. Crooks, L.C. Seefeldt, K.L. Bren, R.M. Bullock, M.Y. Darensbourg, P.L. Holland, B. Hoffman, M.J. Janik, A.K. Jones, M.G. Kanatzidis, P. King, K.M. Lancaster, S.V. Lymar, P. Pfromm, W.F. Schneider, R.R. Schrock, Beyond fossil fuel-driven nitrogen transformations. Science **360**(6391), 1–7 (2018)
2. L. Wang, M. Xia, H. Wang, K. Huang, C. Qian, C.T. Maravelias, G.A. Ozin, Greening ammonia toward the solar ammonia refinery. Joule **2**(6), 1055–1074 (2018)
3. W.E. Jan, G. James, A.S. Mark, K. Zbigniew, W. Winiwarter, How a century of ammonia synthesis inferences the world. Nat. Geosci. **1**, 636–639 (2008)
4. F. Jiao, B. Xu, Electrochemical ammonia synthesis and ammonia fuel cells. Adv. Mater. **31**(31), 1805173 (2019)
5. N. Cao, Z. Chen, K. Zang, J. Xu, J. Zhong, J. Luo, X. Xu, G. Zheng, Doping strain induced bi-Ti^{3+} pairs for efficient N_2 activation and electrocatalytic fixation. Nat. Commun. **10**, 2877 (2019)
6. S.L. Foster, S.I.P. Bakovic, R.D. Duda, S. Maheshwari, R.D. Milton, S.D. Minteer, M.J. Janik, J.N. Renner, L.F. Greenlee, Catalysts for nitrogen reduction to ammonia. Nat. Catal. **1**(7), 490–500 (2018)
7. D. Zhu, L. Zhang, R.E. Ruther, R.J. Hamers, Photo-illuminated diamond as a solid-state source of solvated electrons in water for nitrogen reduction. Nat. Mater. **12**(9), 836–841 (2013)
8. X. Cui, C. Tang, Q. Zhang, A review of electrocatalytic reduction of dinitrogen to ammonia under ambient conditions. Adv. Energy Mater. **8**(22), 1800369 (2018)
9. Y. Ding, L. Huang, J. Zhang, A. Guan, Q. Wang, L. Qian, L. Zhang, G. Zheng, Ru-doped, oxygen-vacancy-containing CeO_2 nanorods toward N_2 electroreduction. J. Mater. Chem. A **8**, 7229–7234 (2020)
10. Z. Wang, X. Wu, Y. Qin, Y. Han, D. Zhang, H. Zhao, J. Chi, G. Xu, M. Wang, S. Li, D. Wang, J. Lai, L. Wang, Efficient nitrogen reduction to ammonia by fluorine vacancies with a multi-step promoting effect. J. Mater. Chem. A **9**(2), 894–899 (2021)
11. J. Deng, J.A. Iñiguez, C. Liu, Electrocatalytic nitrogen reduction at low temperature. Joule **2**(5), 846–856 (2018)
12. A.R. Singh, B.A. Rohr, J.A. Schwalbe, M. Cargnello, K. Chan, T.F. Jaramillo, I. Chorkendorff, J.K. Nørskov, Electrochemical ammonia synthesis—the selectivity challenge. ACS Catal. **7**(1), 706–709 (2016)
13. Y. Song, T. Wang, J. Sun, Z. Wang, Y. Luo, L. Zhang, H. Ye, X. Sun, Enhanced electrochemical N_2 reduction to NH_3 on reduced graphene oxide by tannic acid modification. ACS Sus. Chem. Eng. **7**(17), 14368–14372 (2019)
14. S. Mukherjee, D.A. Cullen, S. Karakalos, K. Liu, H. Zhang, S. Zhao, H. Xu, K.L. More, G. Wang, G. Wu, Metal-organic framework-derived nitrogen-doped highly disordered carbon for electrochemical ammonia synthesis using N_2 and H_2O in alkaline electrolytes. Nano Energy **48**, 217–226 (2018)
15. K. Liu, J. Fu, L. Zhu, X. Zhang, H. Li, H. Liu, J. Hu, M. Liu, Single-atom transition metals supported on black phosphorene for electrochemical nitrogen reduction. Nanoscale **12**(8), 4903–4908 (2020)
16. H. Jin, C. Guo, X. Liu, J. Liu, A. Vasileff, Y. Jiao, Y. Zheng, S.Z. Qiao, Emerging two-dimensional nanomaterials for electrocatalysis. Chem. Rev. **118**(13), 6337–6408 (2018)
17. M. Naguib, V.N. Mochalin, M.W. Barsoum, Y. Gogotsi, 25th anniversary article: MXenes: a new family of two-dimensional materials. Adv. Mater. **26**(7), 992–1005 (2014)
18. X. Zhan, C. Si, J. Zhou, Z. Sun, MXene and MXene-based composites: synthesis, properties and environment-related applications. Nanoscale Horiz. **5**(2), 235–258 (2020)
19. S.Y. Pang, Y.T. Wong, S. Yuan, Y. Liu, M.K. Tsang, Z. Yang, H. Huang, W.T. Wong, J. Hao, Universal strategy for HF-free facile and rapid synthesis of two-dimensional MXenes as multifunctional energy materials. J. Am. Chem. Soc. **141**(24), 9610–9616 (2019)
20. Y. Gao, Y. Cao, H. Zhuo, X. Sun, Y. Gu, G. Zhuang, S. Deng, X. Zhong, Z. Wei, X. Li, J.-G. Wang, Mo_2TiC_2 MXene: a promising catalyst for electrocatalytic ammonia synthesis. Catal. Today **339**, 120–126 (2020)
21. W. Peng, M. Luo, X. Xu, K. Jiang, M. Peng, D. Chen, T.S. Chan, Y. Tan, Spontaneous atomic ruthenium doping in Mo_2CT_X MXene defects enhances electrocatalytic activity for the nitrogen reduction reaction. Adv. Energy Mater. **10**(25), 2001364 (2020)
22. L. Yu, J. Qin, W. Zhao, Z. Zhang, J. Ke, B. Liu, Advances in two-dimensional MXenes for nitrogen electrocatalytic reduction to ammonia. Inter. J. Photoenergy **2020**, 1–11 (2020)
23. Y. Luo, G.-F. Chen, L. Ding, X. Chen, L.-X. Ding, H. Wang, Efficient electrocatalytic N_2 fixation with MXene under ambient conditions. Joule **3**(1), 279–289 (2019)
24. A.D. Handoko, S.N. Steinmann, Z.W. Seh, Theory-guided materials design: two-dimensional MXenes in electro- and photocatalysis. Nanoscale Horiz. **4**(4), 809–827 (2019)
25. J. Xia, S.-Z. Yang, B. Wang, P. Wu, I. Popovs, H. Li, S. Irle, S. Dai, H. Zhu, Boosting electrosynthesis of ammonia on surface-engineered MXene Ti_3C_2. Nano Energy **72**, 104681 (2020)
26. L.R. Johnson, S. Sridhar, L. Zhang, K.D. Fredrickson, A.S. Raman, J. Jang, C. Leach, A. Padmanabhan, C.C. Price, N.C. Frey, A. Raizada, V. Rajaraman, S.A. Saiprasad, X. Tang, A. Vojvodic, MXene materials for the electrochemical nitrogen reduction—functionalized or not. ACS Catal. **10**(1), 253–264 (2019)
27. B. Anasori, M.R. Lukatskaya, Y. Gogotsi, 2D metal carbides and nitrides (MXenes) for energy storage. Nat. Rev. Mater. **2**(2), 16098 (2017)
28. F. Bu, M.M. Zagho, Y. Ibrahim, B. Ma, A. Elzatahry, D. Zhao, Porous MXenes: synthesis, structures, and applications. Nano Today **30**, 100803 (2020)
29. Y. Guo, T. Wang, Q. Yang, X. Li, H. Li, Y. Wang, T. Jiao, Z. Huang, B. Dong, W. Zhang, J. Fan, C. Zhi, Highly efficient electrochemical reduction of nitrogen to ammonia on surface termination modified $Ti_3C_2T_x$ MXene nanosheets. ACS Nano **14**(7), 9089–9097 (2020)
30. T. Li, X. Yan, L. Huang, J. Li, L. Yao, Q. Zhu, W. Wang, W. Abbas, R. Naz, J. Gu, Q. Liu, W. Zhang, D. Zhang, Fluorine-free $Ti_3C_2T_x$ (T = O, OH) nanosheets (∼50–100 nm) for nitrogen fixation under ambient conditions. J. Mater. Chem. A **7**(24), 14462–14465 (2019)
31. Y. Cheng, L. Wang, Y. Song, Y. Zhang, Deep insights into the exfoliation properties of MAX to MXenes and the hydrogen evolution performances of 2D MXenes. J. Mater. Chem. A **7**(26), 15862–15870 (2019)
32. A.D. Handoko, K.D. Fredrickson, B. Anasori, K.W. Convey, L.R. Johnson, Y. Gogotsi, A. Vojvodic, Z.W. Seh, Tuning the basal plane functionalization of two-dimensional metal carbides (MXenes) To control hydrogen evolution activity. ACS Appl. Energy Mater. **1**(1), 173–180 (2017)

Publisher's Note